

# RF COMMISSIONING OF THE CBETA MAIN LINAC CRYOMODULE\*

N. Banerjee<sup>†</sup>, J. Dobbins, G. Hoffstaetter, R. Kaplan, M. Liepe,  
 C. Miller, P. Quigley, E. Smith, V. Veshcherevich

Cornell Laboratory for Accelerator-Based Sciences and Education, Ithaca, USA

## Abstract

The Cornell BNL ERL Test Accelerator (CBETA) employs a superconducting Main Linac Cryomodule in order to perform multi-turn energy recovery operation. Optimizing the field stability of the low bandwidth SRF cavities in the presence of microphonics with limited available RF power is a challenging task. Despite of this, the Main Linac Cryomodule has been successfully used in CBETA to impart a maximum energy gain of 52 MeV, well above the energy gain requirement of CBETA. In this paper, we describe our RF setup and present an overview of our daily RF turn on procedure including automatic coarse tuning, measurement of DAC and phase offsets. We further detail our microphonics and Lorentz Force Detuning measurements from our most recent run period.

## INTRODUCTION

The Cornell-BNL ERL Test Accelerator (CBETA) [1] project currently being commissioned at Cornell University will be the first high-current multi-turn Energy Recovery Linac(ERL) employing SRF cavities operating at 1.3 GHz in CW mode. The main linac [2] provides a total energy gain of 36 MeV using six 7-cell cavities with a design current exceeding 320 mA. During normal operations of the ERL, we will maintain exact energy balance on each cavity leading to zero beam loading which enables us to use high external quality factors  $Q_{\text{ext}} \sim 6.5 \times 10^7$ . This reduces average power requirements and we use solid state RF amplifiers to drive the cavities. At the same time this makes the RF system very sensitive to cryogenic parameters such as pressure and Helium level regulation. Large microphonics detuning several times the operating bandwidth reduces the field stability which we can achieve with available power. In this paper, we describe our automated RF startup procedures along with measurements of relevant cavity parameters.

In the next section, we describe our high level RF setup with results from initial testing of the Solid State Amplifiers and the circulators. Then we describe the performance of our cryogenic system which we have optimized for stable operations. After this, we describe our semi-automated RF turn-on procedure in detail and finally report our measurements during beam operations over the current commissioning phase.

\* This work was supported by the New York State Energy Research and Development Authority and NSF award DMR-0807731.

<sup>†</sup> nb522@cornell.edu

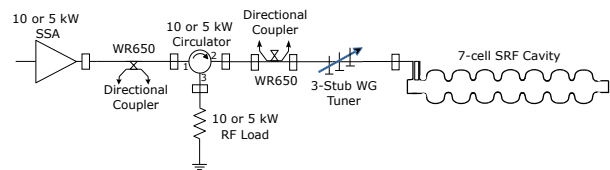


Figure 1: RF power arrangement for one main linac cavity. We inserted a waveguide short between the fundamental power coupler of the 7-cell SRF cavity and the 3-stub waveguide tuner during tests of the solid state amplifiers.

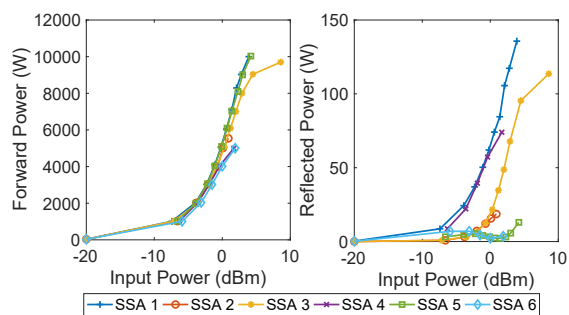


Figure 2: Power transfer function measurement of the 6 solid state amplifiers. While odd numbered amplifiers powering un-stiffened cavities are capable of reaching a forward power of 10 kW, the even numbered ones power the stiffened cavities with a maximum forward power of 5 kW. The left panel shows the forward power as a function of input power, while the right panel shows the power reflected into the SSA from the circulators.

## LINAC SUBSYSTEMS

The Main Linac Cryomodule (MLC) houses six 7-cell SRF cavities optimized for high-current operations with negligible beam loading. All six cavities are operated with a low bandwidth of  $\approx 20$  Hz and are powered by individual Solid State Amplifiers (SSA) from *SigmaPhi* connected through a circulator from *AFT*, directional coupler and a 3-stub waveguide tuner as shown in Fig. 1. There are two sets of high power RF components which are capable of 5 kW and 10 kW for stiffened [3] and un-stiffened cavities respectively. After repairing some manufacturing defects in the circulators and replacing some transistors on one of our SSAs, we tested all these components to full power into a shorted waveguide before connecting them to the cavities. Figure 2 shows the final measurements indicating satisfactory performance of all high power RF components.

The cryogenic system of the MLC is based on the TESLA design. [4] Separate vessels house the six cavities and are supplied liquid Helium through chimneys by the 2 K - 2

Content from this work may be used under the terms of the CC BY 3.0 licence (© 2019). Any distribution of this work must maintain attribution to the author(s), title of the work, publisher, and DOI.

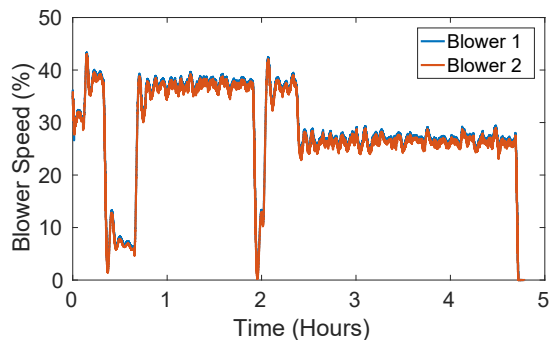


Figure 3: Blower speeds (percentage of maximum) as functions of time during typical 36 MeV RF operations for the FAT.

phase pipe. The pressure exerted on the cavity walls influences the resonant frequency and needs to be regulated. Slow trends in this pressure give rise to very low frequency microphonics detuning ( $\lesssim 1\text{Hz}$ ) and tight cryogenic regulation is necessary during operations. One important indicator of cryogenic performance is the speed of the blowers which regulate the Helium pressure and hence the temperature of the cavity. The data shown in Fig. 3 is within acceptable limits with the two blowers connected to the Helium gas return line never exceeding 50% of maximum speed for nominal energy gain of 36 MeV and both reaching 67.5% at the maximum gain of 52 MeV.

## RF COMMISSIONING AND PERFORMANCE

The initial commissioning of the MLC after setting up the high level RF and cryogenic systems involved calibrations of various signal paths, configuring the Low Level RF (LLRF) system with default parameters and then tuning the cavities to resonance from their warm-up positions. While this process needs to be done only once, we still need a daily start-up procedure to account for various drifts in the machine. In this section we document the approach we follow to prepare the MLC for beam operations. While we have done the initial commissioning manually, most of these steps are automatically executed for routine operations using a dedicated sequencer capable of rudimentary error handling. Such automation has also been used elsewhere [5]. Repeating these procedures everyday ensures stable operations.

**Step 1:** Cavity tuning is the first step towards turn on and we use stepper motor based slow tuners to obtain resonance at the clock frequency of 1299.9 MHz. We use the LLRF system in fixed frequency constant power mode (called Klystron Loop in the Cornell LLRF [6]) to coarse tune the cavity to within a few Hz of resonance on average. During the tuning process, we maximize the field signal while using a forward power of 10 W which gives us the resonance position at an accelerating voltage just above 1.1 MV. The algorithm is based on decision tree approach and is capable of handling the hysteresis of the tuner movement and includes safety

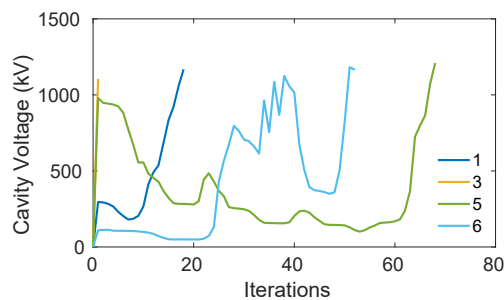


Figure 4: Performance of the automatic coarse tuning algorithm. The graph shows how the accelerating voltage changes as the algorithm progressively tunes four cavities of the main linac to resonance in multiple iterations.

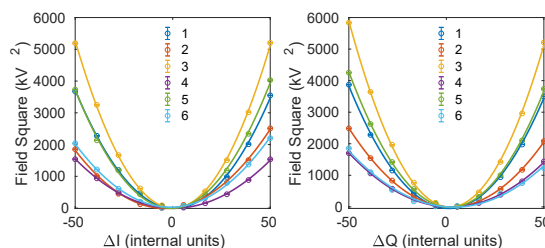


Figure 5: Square of parasitic field inside cavities as functions of change in Digital to Analog Converter (DAC) offsets for in-phase  $\Delta I$  (left panel) and quadrature  $\Delta Q$  (right panel) components of the output phasor. The plots show data for all main linac cavities and the corresponding quadratic fits, with the minima being the computed offsets.

features not to overdrive the tuner. Fig. 4 shows the performance of this algorithm on four cavities illustrating how the algorithm can recover even after going through the resonance peak. This step is a prerequisite for subsequent procedures which requires a well tuned cavity.

**Step 2:** The Digital to Analog Converter (DAC) output used in the LLRF system to drive the vector modulator may have some offset due to manufacturing differences and temperature variations. This leads to some non-zero forward power being injected into the cavity even when the output is set to 0 leading to a parasitic field appearing in the cavity when the feedback loop is not active. To account for the offsets, both the in-phase  $I$  and the quadrature  $Q$  components of the output phasor are shifted by a programmable offset in the LLRF. We measure the square of parasitic field as a function of offset as shown in Fig. 5 setting the optimum value at the position of minimum residual field.

**Step 3:** The LLRF system implements various trips which turn off RF power going into the cavity in case of a situation which might damage the RF system. Setting the various trip parameters is an important step in commissioning the cavities and is automated in our startup sequence. There are three categories of trip parameters which we have to set. The SSA trip parameters set the threshold for the maximum power reflected from the circulator into the SSA. The power

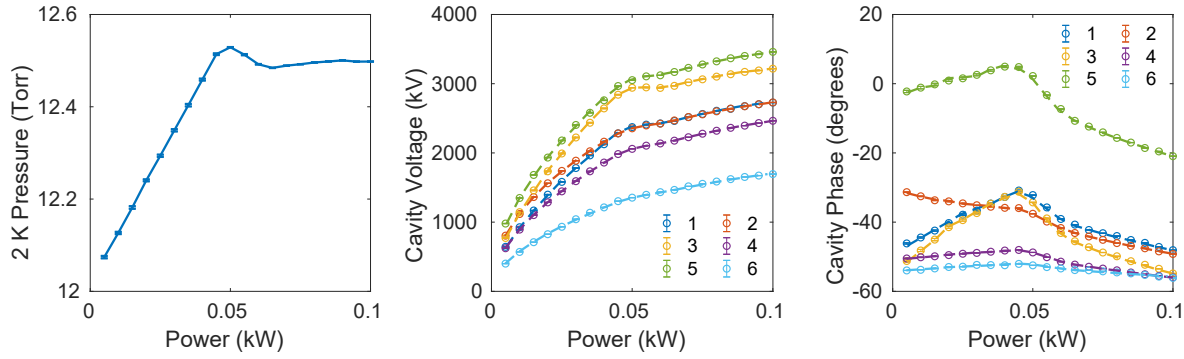


Figure 6: Data recorded to measure field rotation. The first panel shows the change in 2 K pressure as we increase the forward power. The second and the third panel show the voltage and phase as functions of forward power respectively on all cavities. The dashed lines represent fits to models, Eq. (3) and Eq. (4).

scale contains a calibration factor while *Max. power* sets the scaled power threshold. The *Power trip* parameters are thresholds on the maximum forward and reflected power, while quench detection relies on a sudden but sustained fractional decrease in reflected power. Finally, we set the *Field trip* parameters which control the maximum field tolerated by the system during normal operations.

**Step 4:** The phase rotation of the field signal due to the cable length between the field probe and the control system influences the stability of the constant field control loop (called Cavity Loop in the Cornell LLRF). It also directly affects measurement of the tuning angle  $\phi_t \equiv \phi_{\text{Field}} - \phi_{P_f}$  which is the phase difference between the field signal  $\phi_{\text{Field}}$  and the forward power signal  $\phi_{P_f}$ . The detuning  $\delta f$  of the cavity is given by,

$$\delta f = \frac{f_{\text{drive}}}{2Q_L} \tan \phi_t, \quad (1)$$

where  $Q_L$  is the loaded quality factor of the cavity,  $f_{\text{drive}}$  is the clock frequency of the RF system. The average power required by the control system to sustain a voltage  $V$  on a detuned cavity is [7]

$$P \approx \frac{V^2}{8\frac{R}{Q}Q_L} \left[ 1 + \left( \frac{2Q_L\delta f}{f_{\text{drive}}} \right)^2 \right], \quad (2)$$

where  $R/Q$  is the shunt impedance in circuit definition. Substituting Eq. (1) into Eq. (2) and including an unknown phase offset  $\phi_0$ , we get

$$\frac{P}{V^2} = \frac{\sec^2(\phi_{\text{Field}} + \phi_0)}{8\frac{R}{Q}Q_L}. \quad (3)$$

This relation is used to fit cavity voltage and phase data as a function of forward power as illustrated in Fig. 6, with phase offset  $\phi_0$  being one of the fit parameters. Hence, we have incorporated this procedure in our sequencer to set the phase rotation which ensures correct microphonics measurement and optimized field stability.

We can also use this same measurement to characterize the Lorentz Force Detuning (LFD) and pressure sensitivity of

Table 1: Pressure Sensitivity and Lorentz Force Detuning Coefficients as Calculated from Cavity Voltage and Phase Data Shown in Fig. 6.

Cavity	Stiffened	$df/dp$	$K_{\text{LFD}}$
		Hz/Torr	Hz/(MV/m) <sup>2</sup>
1	No	$37.4 \pm 0.6$	$1.52 \pm 0.02$
2	Yes	$18.3 \pm 0.2$	$1.35 \pm 0.01$
3	No	$47.1 \pm 0.4$	$1.41 \pm 0.01$
4	Yes	$17.4 \pm 0.2$	$1.21 \pm 0.01$
5	No	$38.8 \pm 0.4$	$1.30 \pm 0.01$
6	Yes	$11.7 \pm 0.7$	$1.57 \pm 0.08$

the cavities. Once the unknown phase offsets are determined, we can use it calculate net detuning as functions of cavity voltage  $V$  and 2 K pressure  $p$ . Consequently, we can fit the detuning to a model,

$$\delta f = \delta f_0 - K_{\text{LFD}} \frac{V^2}{L^2} + \frac{df}{dp}(p - p_0), \quad (4)$$

where  $\delta f_0$  is a constant offset,  $K_{\text{LFD}}$  is the LFD coefficient,  $L$  is the active length and  $df/dp$  is the pressure sensitivity at the nominal pressure  $p_0 = 12.5$  Torr. Typical results from the fit are summarized in Table 1 which shows that the stiffened cavities are less sensitive to pressure variations while they are equally sensitive to LFD which is consistent with the design.

**Step 5:** Microphonics poses a major constraint on field stability for the MLC cavities which we operate with high  $Q_L$  as noted in the previous section. The LLRF system provides a tool to measure the microphonics in the system as shown in Fig. 7. The LLRF measures the peak forward power and detuning with a time resolution of 10  $\mu\text{sec}$  and 100  $\mu\text{sec}$  respectively. We ensure that the peak microphonics detuning is  $\leq 50\text{Hz}$  for stable operations while the peak power is less than the maximum output of the SSA connected to the cavities, 5 kW for stiffened and 10 kW for un-stiffened. If deemed necessary, we can use the spectrum

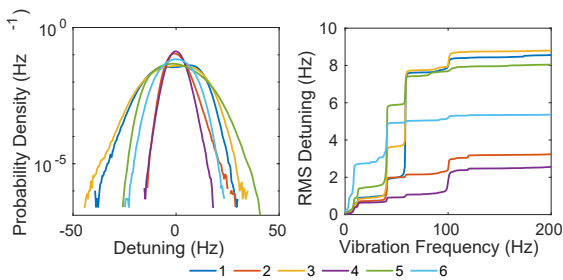


Figure 7: Microphonics measurements on all MLC cavities using the LLRF diagnostic tool. The left panel shows the histogram of detuning while the right panel shows the integrated spectrum.

measurement to determine the frequencies of strong vibrations in the cryomodule and then activate the ANC algorithm on these sources.

**Step 6:** Stability of electric field in the RF cavity depends on the proportional and integral gains of the field control loop (cavity Loop). We complete step 5 with some default parameters for the control loop, namely with a normalized proportional gain of about 100 and a zero integral gain. Then we measure the standard deviation of the field amplitude and phase as a function of the feedback gains in order to optimize the performance of feedback control.

## CONCLUSION

The Main Linac Cryomodule used for energy recovery in CBETA houses six 7-cell SRF cavities with a nominal accelerating voltage of 6 MV each. Three of these cavities are fitted with stiffening rings in order to reduce their sensitivity to external vibrations primarily driven by the cryogenic system. In order to sustain stable field at the required gradient, the un-stiffened cavities are powered by SSAs capable of generating 10 kW while the others use 5 kW sources. While initial testing of the high power RF components revealed some manufacturing defects, after repair all components operate normally and we have tested everything to full power. We also carefully optimized various cryogenic system control loops which regulate Helium level and pressure inside the cryomodule in response to varying levels of thermal load during RF operations. The performance of the room temperature Helium blowers which maintain 2 K vapour pressure inside the cryomodule strongly suggests that the thermal dissipation of the cavities is within the expected range.

The initial RF system commissioning involved calibrating the signal paths, tuning the cavities back from their warm-up positions and preparing the LLRF control. Once the system was sufficiently optimized in the initial days of operations, we have automated turn on procedure which is now run by a sequencer everyday before starting beam operations. We start by tuning the cavities to resonance using the slow tuner system, followed by reducing the leakage of forward power

into the cavities by optimizing the offsets of the LLRF DACs. Then we set the parameters which allow the LLRF to safely trip off, protecting the system from permanent damage. After this, we measure the field rotation offset by measuring the average cavity voltage and phase as functions of forward power. Finally we measure microphonics and field stability and optimize the field and resonance control loops for stable operations. Future work will involve automating steps 5 and 6 of the startup procedure with special emphasis on establishing stable high-current energy recovery operations with no spontaneous trips or long term drifts.

## ACKNOWLEDGEMENTS

We would like to thank Dan Sabol and Colby Shore for setting up the cryogenic systems for both cryomodules and help in optimizing the Helium control loops. We would also like to acknowledge Adam Bartnik, Colwyn Gulliford and Kirsten Deitrick for devoting a substantial amount of time towards operations. This work was supported by the New York State Energy Research and Development Authority while the CLASSE facilities are operated with major support from the National Science Foundation. Nilanjan would like to thank the organizing committee of the SRF workshop for providing travel support.

## REFERENCES

- [1] G. H. Hoffstaetter *et al.*, “CBETA, the 4-Turn ERL with SRF and Single Return Loop”, in *Proc. 9th Int. Particle Accelerator Conf. (IPAC'18)*, Vancouver, Canada, Apr.-May 2018, pp. 635–639. doi:10.18429/JACoW-IPAC2018-TUYGBE2
- [2] F. Furuta *et al.*, “Performance of the Novel Cornell ERL Main Linac Prototype Cryomodule”, in *Proc. 28th Linear Accelerator Conf. (LINAC'16)*, East Lansing, MI, USA, Sep. 2016, pp. 492–495. doi:10.18429/JACoW-LINAC2016-TUPLR011
- [3] S. Posen and M. Liepe, “Mechanical optimization of superconducting cavities in continuous wave operation”, *Phys. Rev. ST Accel. Beams*, vol. 15, p. 022002, Feb. 2012.
- [4] E. N. Smith, Y. He, G. H. Hoffstaetter, M. Liepe, and M. Tigner, “Cryogenic Distribution System for the Proposed Cornell ERL Main Linac”, in *Proc. 3rd Int. Particle Accelerator Conf. (IPAC'12)*, New Orleans, LA, USA, May 2012, paper MOPPP026, pp. 619–621.
- [5] Z. Q. Geng, “RF Control Optimization and Automation for Normal Conducting Linear Accelerators”, *IEEE Transactions on Nuclear Science*, vol. 64, no. 8, pp. 2361–2368, Aug. 2017.
- [6] A. Neumann *et al.*, “CW Measurements of Cornell LLRF System at HoBiCaT”, in *Proc. SRF'11*, Chicago, IL, USA, Jul. 2011, paper MOP0067, pp. 262–266.
- [7] M. Liepe and S. Belomestnykh, “RF Parameter and Field Stability Requirements for the Cornell ERL Prototype”, in *Proc. PAC'03*, Portland, OR, USA, May 2003, paper TPAB056, pp. 1329–1331.